HAL
open science

Response of Mars O+ pickup ions to the 8 March 2015 ICME: Inferences from MAVEN data-based models

Shannon M. Curry, Janet G. Luhmann, Yingjuan J. Ma, Chuanfei F. Dong, David A. Brain, François Leblanc, Ronan Modolo, Yaxue Dong, James P. Mcfadden, Jasper S. Halekas, et al.

To cite this version:

Shannon M. Curry, Janet G. Luhmann, Yingjuan J. Ma, Chuanfei F. Dong, David A. Brain, et al.. Response of Mars O+ pickup ions to the 8 March 2015 ICME: Inferences from MAVEN data-based models. Geophysical Research Letters, 2015, 42 (21), pp.9095-9102. 10.1002/2015GL065304 . insu-01238391

HAL Id: insu-01238391

https://insu.hal.science/insu-01238391v1

Submitted on 17 Jul 2020

HAL is a multi-disciplinary open access archive for the deposit and dissemination of scientific research documents, whether they are published or not. The documents may come from teaching and research institutions in France or abroad, or from public or private research centers.

L'archive ouverte pluridisciplinaire **HAL**, est destinée au dépôt et à la diffusion de documents scientifiques de niveau recherche, publiés ou non, émanant des établissements d'enseignement et de recherche français ou étrangers, des laboratoires publics ou privés.

AGU PUBLICATIONS

Geophysical Research Letters

RESEARCH LETTER
10.1002/2015GL065304

Special Section:
First Results from the MAVEN Mission to Mars

Key Points:
- The shock phase of an ICME drives the most ion escape at Mars
- The shock phase of an ICME has an O^+ escape rate of 4.1e25/s
- O sputtering from the shock phase of an ICME may be on the order of 1e26/s

Correspondence to:
S. M. Curry,
smcurry@umich.edu

Citation:
Curry, S. M., et al. (2015), Response of Mars O^+ pickup ions to the 8 March 2015 ICME: Inferences from MAVEN data-based models, *Geophys. Res. Lett.*, *42*, 9095–9102, doi:10.1002/2015GL065304.

Received 21 JUL 2015
Accepted 15 SEP 2015
Published online 5 NOV 2015

©2015. American Geophysical Union. All Rights Reserved.

Response of Mars O^+ pickup ions to the 8 March 2015 ICME: Inferences from MAVEN data-based models

S. M. Curry[1], J. G. Luhmann[1], Y. J. Ma[2], C. F. Dong[3], D. Brain[4], F. Leblanc[5], R. Modolo[5], Y. Dong[4], J. McFadden[1], J. Halekas[6], J. Connerney[7], J. Espley[7], T. Hara[1], Y. Harada[1], C. Lee[1], X. Fang[4], and B. Jakosky[4]

[1]Space Sciences Laboratory, University of California, Berkeley, California, USA, [2]Institute of Geophysics and Planetary Physics, University of California, Los Angeles, California, USA, [3]Deptartment of Atmosphere, Oceanic and Space Sciences, University of Michigan, Ann Arbor, Michigan, USA, [4]Laboratory for Atmospheric and Space Physics, University of Colorado Boulder, Boulder, Colorado, USA, [5]LATMOS, UVSQ, Guyancourt, France, [6]Department of Physics and Astronomy, University of Iowa, Iowa City, Iowa, USA, [7]NASA Goddard Space Flight Center, Greenbelt, Maryland, USA

Abstract We simulate and compare three phases of the Mars-solar wind interaction with the 8 March interplanetary coronal mass ejection (ICME) event using Mars Atmosphere and Volatile EvolutioN (MAVEN) mission observations in order to derive heavy ion precipitation and escape rates. The MAVEN observations provide the initial conditions for three steady state MHD model cases, which reproduce the observed features in the solar wind density, velocity, and magnetic field seen along the MAVEN orbit. Applying the MHD results to a kinetic test particle model, we simulate global precipitation and escape maps of O^+ during the (1) pre-ICME phase, (2) sheath phase, and (3) ejecta phase. We find that the Case 1 had the lowest precipitation and escape rates of 9.5×10^{25} and $4.1\times10^{25}\,s^{-1}$, Case 2 had the highest rates of 9.5×10^{25} and $4.1\times10^{25}\,s^{-1}$, and Case 3 had rates of 3.2×10^{25} and $1.3\times10^{25}\,s^{-1}$, respectively. Additionally, Case 2 produced a high-energy escaping plume >10 keV, which mirrored corresponding STATIC observations.

1. Introduction

On 8 March 2015 at ~15:20 UT, MAVEN observed the passage of an interplanetary coronal mass ejection (ICME) at Mars that drove a significant response from Mars' atmosphere and plasma environment [*Jakosky et al.*, 2015]. ICMEs are solar transients typically lasting 1–2 days consisting of several phases that can be observed in the solar wind: the sheath, the plasma sheath, and the cloud or ejecta. Each phase is marked by different observable indicators, including enhancements of the solar wind density, velocity, dynamic pressure, and strong rotations in the interplanetary magnetic field (IMF) [*Rouillard et al.*, 2009; *Prise et al.*, 2015].

The interaction of an ICME with Mars' atmosphere is markedly different than with that of Earth's due to the lack of a global dipole magnetic field [*Crider et al.*, 2005; *Futaana et al.*, 2006; *Haider et al.*, 2009]. A limited number of data studies have investigated the influence of ICMEs on Mars' plasma environment due to the occurrence rate of solar events as well as observational constraints [*Opgenoorth et al.*, 2013]. However, some of these results suggest that the response includes enhanced atmospheric ion escape [e.g., *Edberg et al.*, 2011].

During nominal solar wind conditions, pickup ions play a major role in atmospheric escape at weakly magnetized planets, such as Mars and Venus, so during an ICME, the response of pickup ions to such extreme conditions is a subject of great interest [e.g., *Dubinin et al.*, 2011, and references therein]. Pickup ions are formed when the solar wind directly interacts with the upper atmosphere, and newly created ions can be picked up and swept away by the background convection electric field. They can directly escape [*Brain et al.*, 2015; *Y. Dong et al.*, 2015] or precipitate back into the atmosphere and induce atmospheric sputtering of neutrals. Sputtering is believed to be one of the main drivers of atmospheric escape during the early epochs of our solar system when the solar activity and EUV intensities were much higher than the present day [*Luhmann et al.*, 1992; *Leblanc and Johnson*, 2002; *Leblanc et al.*, 2015].

In this paper, we present a modeling study of the global ion precipitation and escape based on MAVEN data during three periods of the 8 March 2015 ICME. Section 2 will discuss the observations motivating this study, Section 3 will discuss the suite of models for the study, section 4 will present results, and we summarize the conclusions in section 5.

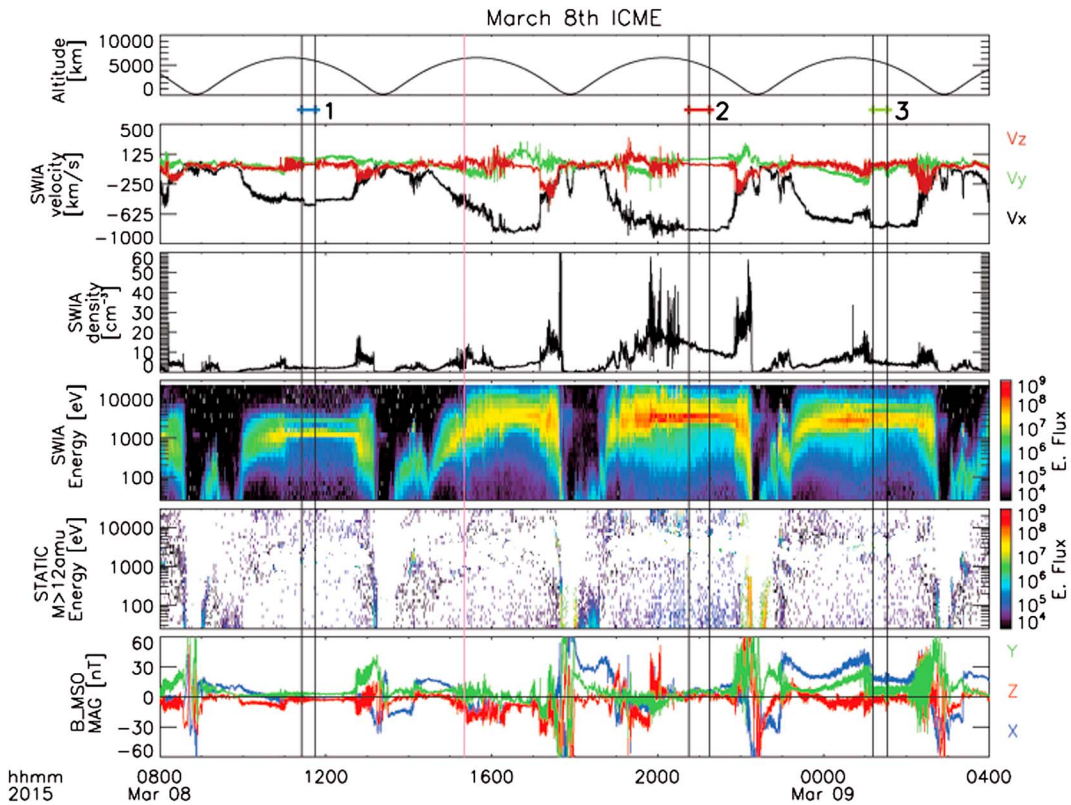

Figure 1. MAVEN observations of the 8 March 2015 ICME. From top to bottom: MAVEN spacecraft altitude in kilometers, the solar wind velocity in km/s as measured by SWIA, the solar wind density in cm^{-3} as measured by SWIA, an energy spectrogram of the ions observed by SWIA in energy flux (eV/(eV cm^{-2} s sr)), an energy spectrogram of heavy ions (amu > 12) observed by STATIC in energy flux (eV/(eV cm^{-2} s sr)), and the magnetic field in MSO coordinates as measured by MAG (nT). The three time periods selected for data-model comparisons were (1) 8 March 2015/11:30–11:40, (2) 8 March 2015/20:45–21:15, and (3) 9 March 2015/01:10–01:30 in UTC, outlined in black lines with the arrival of the ICME ~15:20 marked in the pink line.

2. Measurements

For the ICME observations, we focused on the plasma and field instruments aboard MAVEN, which began its primary science mission on 16 November 2014. For the ion observations, we used The Suprathermal and Thermal Ion Composition (STATIC) [*McFadden et al.*, 2014] and the Solar Wind Ion Analyzer (SWIA) [*Halekas et al.*, 2015]. STATIC measures the ions' energy over a range of 0.1 eV/q–30 keV/q and mass from 1 to 70 amu/q that distinguishes the main ion species: O_2^+, CO_2^+, and O^+. SWIA is an energy and angular ion spectrometer covering an energy range between 5 eV/q and 25 keV/q with 48 energy steps logarithmically spaced. Additionally, this study uses measurements from the Magnetometer (MAG) instrument, which has an intrinsic rate of 32-vector samples per second [*Connerney et al.*, 2014]. The IMF observations are presented in a Cartesian coordinate system corresponding to the Mars Solar Orbital scheme (MSO). The system is centered at Mars where X_{MSO} points toward the Sun, Y_{MSO} is aligned with the dusk direction, and Z_{MSO} completes the right-hand system.

3. Models and Inputs

As discussed in *Jakosky et al.* [2015], the 8 March ICME has been the strongest solar event observed to date by MAVEN. At ~15:20 UTC 8 March 2015, MAG observed a strong enhancement and rotation in the magnetic field, accompanied by an increase in solar wind velocity and ion fluxes that are typically associated with the arrival of an ICME. The IMF returned to its nominal value, ~3 nT, roughly 48 h later. We have selected three "snapshots" or cases on 8 and 9 March that represent the solar wind and Mars space environment (1) before the ICME passage, (2) during the ICME sheath phase, and (3) during the ICME ejecta phase.

Table 1. The Three Snapshots of the 8 March 2015 ICME That Are Compared With MHD and Test Particle Simulation Results[a]

Case	Time Period	N_{SW} (cm^{-3})	U_{SW} (km/s)	B_{IMF} (nT)	Precipitation (s^{-1})	Escape (s^{-1})
1	3/8/2015 11:30–11:40	1.8	(−505, 15, −10)	(−2.5, 2.8, −1.0)	1.2e25	3.7e24
2	3/8/2015 20:45–21:15	11	(−825, 63, −6)	(5.2, 5.4, 1.7)	9.5e25	4.1e25
3	3/9/2015 01:10–01:30	4.5	(−780, −45, −10)	(19.1, 7.6, −0.8)	3.2e25	1.3e25

[a]Case 1 corresponds to the pre-ICME conditions, Case 2 corresponds to the sheath phase, and Case 3 corresponds to the ejecta phase. From left to right: the time period in UTC, the solar wind proton density (cm^{-3}), the solar wind velocity in MSO coordinates (km/s), the ion temperature (eV), the IMF field components in MSO coordinate (nT), and the O^+ precipitation and escape rates (s^{-1}). Dates are formatted as month/day/year.

Figure 1 illustrates the progression of the ICME passage from 8 to 9 March using SWIA, STATIC, and MAG. Before the ICME, SWIA measured a solar wind proton density of 1.8 cm^{-3}, a flow speed of 505 km/s, and IMF of 4.8 nT (Case 1), representing nominal solar wind conditions. Following the arrival of the ICME at ~15:20 UTC, MAVEN observed the sheath phase with a dramatic increase in the upstream proton density to 11 cm^{-3}, a solar wind velocity to 825 km/s, and IMF of 7.8 nT (Case 2). During the sheath, SWIA observed an increase in the energy flux by almost 2 orders of magnitude, while STATIC observed higher fluxes of both low- and high-energy heavy ions (<100 eV and >4 keV). MAG observed strong magnetic field rotations and compressions after the onset of the 8 March ICME, as are typically associated with the sheath region produced by an ICME. Finally, during the ejecta phase (Case 3), the solar wind proton density was measured at 4.5 cm^{-3} and the flow speed at 780 km/s with an IMF of 20.5 nT. SWIA observed an enhancement in the solar wind protons, but less so than during the sheath phase while MAG observed much stronger magnetic field rotations than during the sheath phase. It should be noted that proton stragglers in the STATIC data were removed from ~1 keV to 3 keV as they not physical or representative of the O^+ pickup ions.

Using the solar wind conditions during these three ICME phases as initial boundary conditions and inputs, we calculated three corresponding steady state simulations of the Mars space environment using a multispecies magnetohydrodynamic (MHD) model [*Ma et al*., 2015]. The MHD model is a multispecies single-fluid model of Mars, using the University of Michigan BATS-R-US code [*Powell et al*., 1999; *Ma et al*., 2004]. The model self-consistently solves four continuity equations to track the mass densities of H^+, O^+, O_2^+, and CO_2^+, where all ion species share the same velocity and temperature. Crustal magnetic fields are included in the simulation using an *Arkani-Hamed* [2001] spherical harmonic scheme, positioned at dusk, night, and dawn based on the periapsis time of orbits during each case. Additionally, ion-neutral collisions and major chemical reactions are included in the simulation. It should be noted that the solar wind and IMF inputs for the MHD cases are based on the average of the selected time periods in Table 1.

In order to validate the MHD model, we compare the MHD model results for the 8 March 2015 ICME with both the solar wind velocity and the magnetic field as measured by MAVEN, seen in Figure 2. For additional data-model comparisons, we refer readers to a companion study by C. *Dong et al.* [2015], focusing on the multifluid MHD simulation of the same ICME event. In Case 1 (Figure 2a), the solar wind inputs were based on the conditions from 11:20 to 11:30 (see Table 1). The MHD fields show the best agreement with the bulk flow as measured by SWIA (top) and magnetic field as measured by MAG (bottom) up until the onset of the ICME at ~15:20. In Case 2 (Figure 2b), the solar wind inputs were based on the conditions from 20:45 to 11:15 and the simulation results again show strong agreement during the sheath phase of the ICME, with significant enhancements of the magnetic field and solar wind velocities. Finally, the Case 3 ejecta phase based on the average solar wind conditions from 1:10 to 1:30 also show good agreement with the main ICME features, particularly as the density drops while as the high magnetic field rotations and solar wind velocities continue to propagate.

Because the MHD results capture the main features of the observed ICME, we can use the steady state solutions as the background fields and apply them to the Mars Test Particle (MTP) simulation. The MTP is a kinetic test particle simulation that follows the trajectories of particles of any atomic weight through the Mars space environment. The MTP is a collisionless 3-D Monte Carlo model that randomly assigns the particles' initial position, energy, and direction. Additional details of the model can be found in *Fang et al*. [2008] and *Curry et al*. [2013, 2015]. The MTP simulation tracks the trajectories of the particles without any implicit averaging of the gyration or pitch angle of the particles. Consequently, a kinetic approach to modeling the ions in the Mars space environment provides an important tool for constructing global maps of the ion precipitation and escape during multiple phases of an ICME.

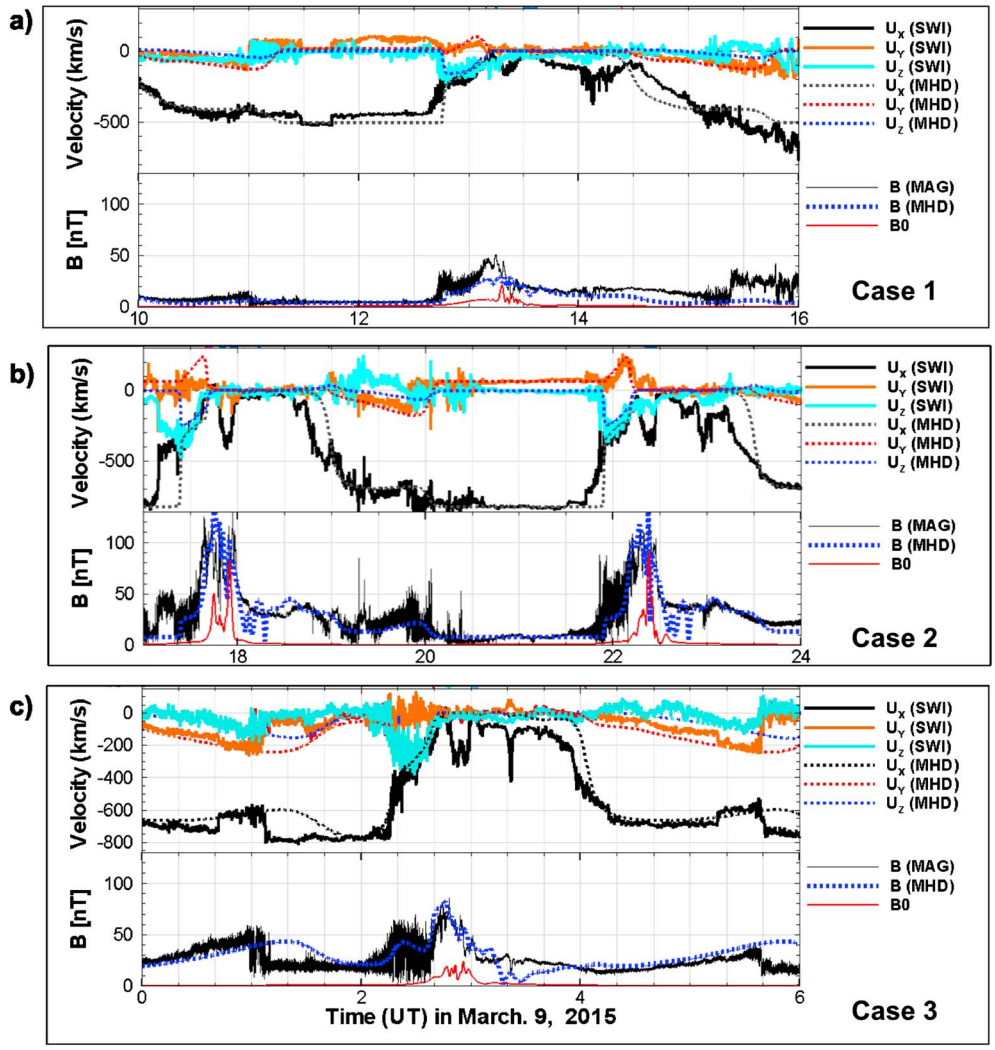

Figure 2. Data-model comparisons of the multispecies MHD model [*Ma et al.*, 2004, 2015] with MAVEN observations of the solar wind and IMF using SWIA and MAG, respectively. (a) Case 1 comparisons of the (top) solar wind velocity and (bottom) magnetic field. The dashed lines represent the MHD simulation and the solid lines represent MAVEN observations for the specified components. Cases (b) 2 and (c) 3 are compared similarly.

4. Results

The MTP uses an inner boundary of 300 km and an outer boundary of 4 R_M to represent the altitude of O^+ precipitation and escape, respectively. Figure 3 illustrates the MTP simulation results for O^+ pickup ion precipitation for each phase of the 8 March 2015 ICME, with the O^+ flux on the top row and the average energy per particle on the bottom row (both log scale). In Case 1 where the ICME has not yet arrived at Mars, the southern hemisphere and dawnside of Mars (~60° east, ~60° south) exhibit the highest flux of O^+ precipitation, with other localized peaks near the 300 km equatorial region. The highest energy, in the ≥1 keV range, also corresponds to the southern hemisphere and dawnside, as would be expected for this IMF configuration (roughly corresponding to an away sector Parker spiral) [*Curry et al.*, 2015]. The precipitation rate for Case 1 is $1.2 \times 10^{25}\ s^{-1}$, as listed in Table 1.

In Case 2, there is still a high-flux, high-energy source of O^+ precipitation in the southern hemisphere, but there is additional high-flux, high-energy O^+ precipitation in the northern hemisphere near dawn and the dayside (~30° west, ~30° north, and ≥~50° north, respectively). Case 2 represents the sheath phase of the ICME that is extremely turbulent, with high solar wind density, temperature, and bulk velocity as well as a rotation in the magnetic field (Figure 1). These conditions create a scenario where the dayside ionosphere

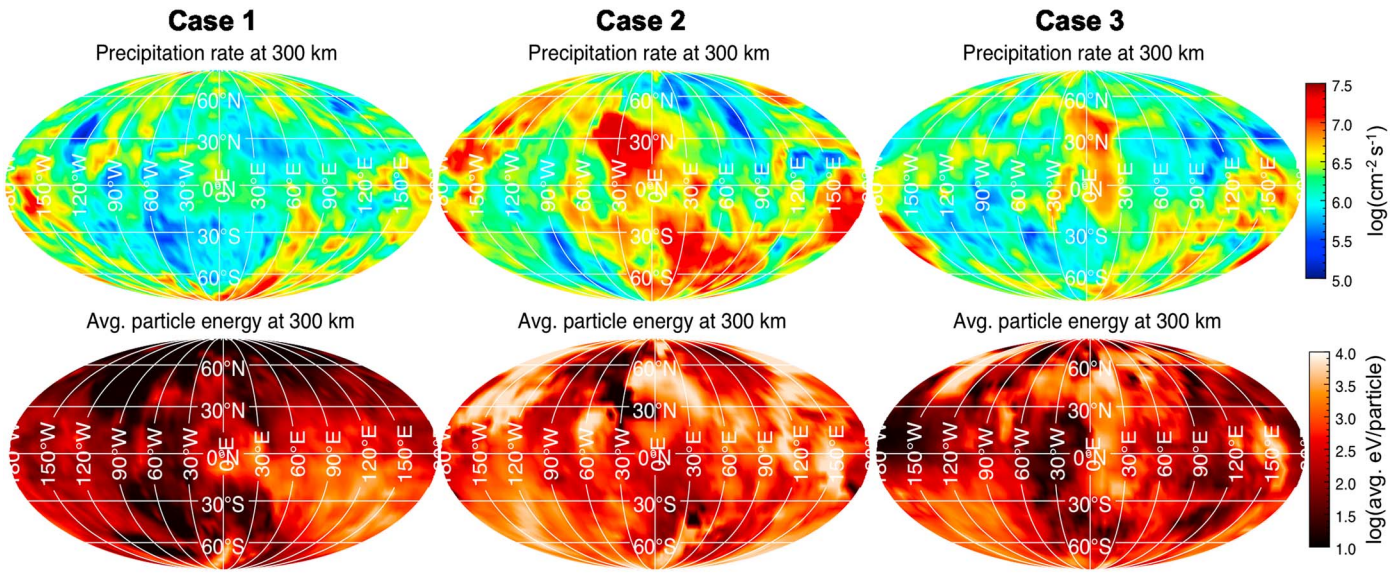

Figure 3. Pickup ion maps of O^+ precipitation on a 300 km shell around Mars modeled by the MTP simulation. (top row) Mollweide projections (MSO) of precipitation flux ($cm^{-2}\,s^{-1}$, log scale) for Cases 1–3 (left to right). (bottom row) Mollweide projections (MSO) of the average energy per particle flux (log scale, average eV/particle) for Cases 1–3 (left to right). 0°N/S, 0°E/W represents downtail, where 90° west is duskward and 90° east is dawnward.

is compressed and bombarded with an increased proton flux causing a dramatic increase in ion production. Consequently, there is a sharp increase in O^+ precipitation on the dayside and throughout the northern hemisphere. In fact, the dayside and northern hemisphere also have the highest-energy deposition, with the average particle energy exceeding 10 keV. This contributes directly to an increase in the precipitation rate almost an order of magnitude for Case 2 to $9.5 \times 10^{25}\,s^{-1}$.

As the passage of the ICME progresses, MAVEN observed the ejecta phase, represented by Case 3. The solar wind velocity is extremely high at 780 km/s with an IMF of ~20 nT, which is the highest magnetic field observed by the MAVEN mission to date. But during the ejecta phase, the solar wind density drops, which in turn lowers the ion production. Figure 2c reflects this with slightly lower O^+ fluxes compared to Case 2, but still enhanced in comparison to Case 1 before the ICME. The highest flux is mostly on the nightside, but the highest-energy particles appear to precipitate in the northern hemisphere again. The precipitation rate for Case 3 is still higher than the pre-ICME precipitation in Case 1 but has decreased to $3.2 \times 10^{25}\,s^{-1}$. This is an important result as it suggests that the heaviest O^+ precipitation is during the sheath phase of the ICME rather than the ejecta phase. Again, heavy ion precipitation is the primary driver of sputtering and *Wang et al.* [2014] calculated the sputtered escape rate of O for extreme cases, such as the sheath phase of the ICME simulated here, to be $1 \times 10^{26}\,s^{-1}$. The precipitation rate in the *Wang et al.* [2014] study was $8.7 \times 10^{25}\,s^{-1}$, and for reference, Case 2 had a precipitation rate of $9.5 \times 10^{25}\,s^{-1}$.

With respect to the direct atmospheric loss at Mars, Figure 4 illustrates the O^+ particles escaping from a 4 R_M shell around the planet. Case 1 exhibits the canonical tailward loss, which is in the low-energy range of 0–100 eV, and plume loss, which is in the high-energy range of $\geq$10 keV. The fin-like shape of the plume on the duskside (~60° west, ~30–60° north) is a stream of ions being accelerated by the background convective electric field and is consistent with an away sector Parker spiral [*Curry et al.*, 2014]. The O^+ escape rate is $3.7 \times 10^{24}\,s^{-1}$ (0.1 kg/s), showing good agreement with other modeling and observational studies during nominal solar wind conditions [e.g., *Brain et al.*, 2010; *Dubinin et al.*, 2011].

The escape pattern for Case 2 during the sheath phase of the ICME is markedly different than Case 1, as seen in Figure 4 (middle column). While the high-flux, low-energy tail still appears, the plume has intensified in flux in the northern hemisphere while simultaneously exhibiting a new stream of O^+ escape across the dawn section of the northern and southern hemispheres (~60–120° east). This constitutes the highest-energy channel of escape at $\geq$30 keV. Using a different test particle model to simulate pickup ions, *Rahmati et al.* [2015] predicted O^+ in the 25–100 keV range for the 8 March 2015 ICME. Incidentally, solar energetic particles

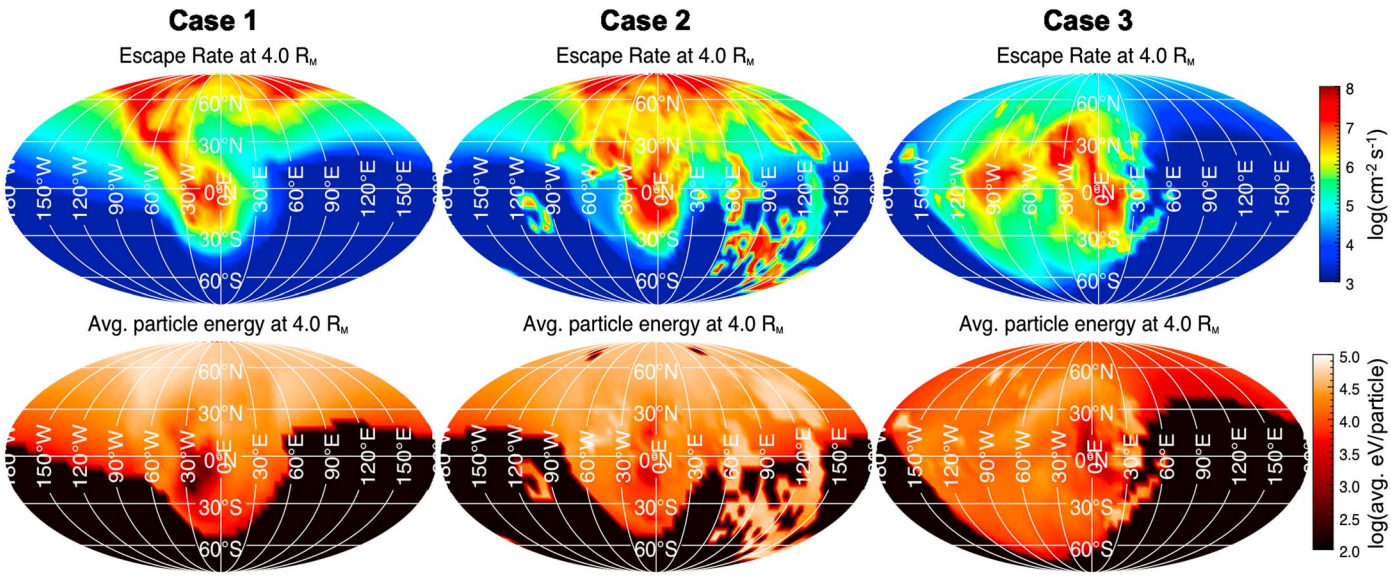

Figure 4. Pickup ion maps of O^+ escape from a 4 R_M shell around Mars modeled by the MTP simulation. (top row) Mollweide projections (MSO) of O^+ precipitation flux ($cm^{-2}\,s^{-1}$, log scale) for Cases 1–3 (left to right). (bottom row) Mollweide projections (MSO) of the average energy per particle flux (log scale, average eV/particle) for Cases 1–3 (left to right). 0°N/S, 0°E/W represents downtail, where 90° west is duskward and 90° east is dawnward.

also observed 10–100 keV O^+ ions during the ICME as seen in Figure 1. As with the precipitation rates, the simulated O^+ escape rate for the sheath phase of the ICME is over an order of magnitude higher than Case 1 at $4.1 \times 10^{25}\,s^{-1}$ (1.1 kg/s).

Finally, the O^+ escape during Case 3 shows a clear shift in the plume to the equatorial region. Indeed, Case 3 exemplifies why this high-energy population of escaping ions is not, in fact, a "polar plume" but rather a "high-energy plume" as it follows the convective electric field, $E = -U \times B$. Since the IMF is typically draped in a Parker spiral configuration [*Brain et al.*, 2006], the plume is typically in the northern or southern polar region but a strong B_{XMSO} or B_{ZMSO} component can rotate the +E field, as seen in Case 3 where the high-flux, high-energy population of O^+ is in the duskward equatorial plane. The escape rate in Case 3 mirrors the trend seen in the precipitation rates where there is less escaping O^+ during the ejecta phase than the sheath phase, but the escape in Case 3 is still significantly higher than in Case 1. The O^+ escape rate for the ejecta phase of the ICME designated by Case 3 is $1.3 \times 10^{25}\,s^{-1}$ (0.4 kg/s).

Using MAVEN observations as inputs for simulating three phases of the 8 March ICME, we find that the sheath phase of the ICME drives the most significant heavy ion precipitation and escape. Figure 5 illustrates a comparison of the STATIC heavy ion spectra and the MTP O^+ spectra during the sheath phase of the ICME (Case 2). STATIC observed an enhancement of high-energy pickup ions in the 1–10 keV range, with peak fluxes of O^+, O_2^+, and CO_2^+ in the 10–25 keV range, which is the instrument's upper energy limit (STATIC data were masked from 1 keV to 5 keV in order to remove stragglers). The STATIC- and MTP-simulated spectra show strong agreement during the sheath phase, capturing the peak near 10 keV followed by a decrease and increase again in flux near 25 keV. This suggests that the sheath phase not only dominates the precipitation and escape rates but also enhances the high-energy, heavy ion flux. This has major implications for understanding how Mars' atmosphere responds to the passage of an ICME and how our Sun during an earlier, more active epochs of our solar system may have driven atmospheric escape via ion loss and sputtering.

5. Conclusion

We present the response of pickup ions to the 8 March ICME event using MAVEN data and a test particle simulation. We used the multispecies MHD model for the background fields of the MTP, which reproduced the major features of the ICME observed by MAVEN. Following, we applied the MTP to create global maps of O^+ precipitation and escape during three distinct cases that represent the Mars space environment over

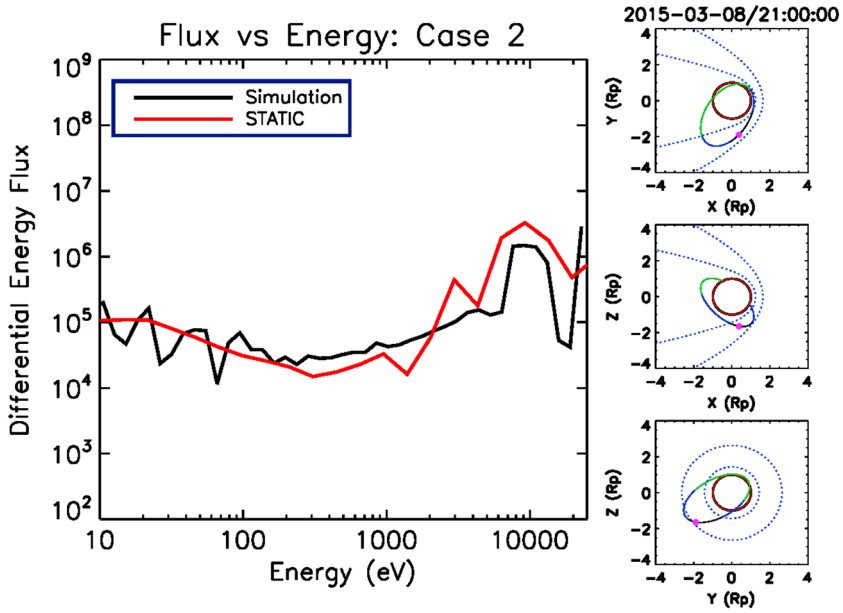

Figure 5. (left) Flux versus energy comparison of STATIC heavy ion spectra averaged over the Case 2 time range with a midpoint of 21:00 (red) and the MTP O^+ spectra (black) in differential energy flux (eV cm^{-2} s^{-1} eV^{-1} sr^{-1}). (right) MAVEN orbit projections of the spacecraft at 21:00 UTC (Case 2 midpoint) in the *XY*, *XZ*, and *YZ* planes (MSO coordinates).

the passage of the ICME: (1) the pre-ICME phase, (2) the sheath phase, and (3) the ejecta phase. The pre-ICME phase, Case 1, was based on nominal solar wind conditions and was consistent with both observed and predicted precipitation and escape rates. The sheath phase, Case 2, had the highest solar wind velocity and density as observed by SWIA and consequently had the highest precipitation and escape rates. Additionally, the simulation of the sheath phase produced a high-energy plume as well as a beam of >30 keV ions, which were mirrored in corresponding STATIC observations. Finally, the ejecta phase, Case 3, had the highest observed magnitude field but lower solar wind density, which was manifested in a lower precipitation rate. The O^+ escape rate during the ejecta phase was also lower, but the map of the simulated escape showed a scenario where the plume was in the duskward equatorial plane, rather than the pole. The consistency of the escaping pickup ion observations with the models supports the future uses of the models for both global and historical extrapolations of ion escape from Mars.

Acknowledgments
The MAVEN project is supported by NASA through the Mars Exploration Program, and MAVEN data are publicly available through the Planetary Data System. This research would not be possible without the diligent efforts of the spacecraft and instrument teams over many years. Additionally, the authors would like to thank Andrew Poppe and Christina Lee for their support.

The Editor thanks two anonymous reviewers for their assistance in evaluating this paper.

References

Arkani-Hamed, J. (2001), A 50-degree spherical harmonic model of the magnetic field of Mars, *J. Geophys. Res.*, *106*, 23,197–23,208, doi:10.1029/2000JE001365.

Brain, D., D. Mitchell, and J. Halekas (2006), The magnetic field draping direction at Mars from April 1999 through August 2004, *Icarus*, *182*(2), 464–473, doi:10.1016/j.icarus.2005.09.023.

Brain, D., et al. (2010), A comparison of global models for the solar wind interaction with Mars, *Icarus*, *206*(1), 139–151, doi:10.1016/j.icarus.2009.06.030.

Brain, D. A., et al. (2015), The spatial distribution of planetary ion fluxes near Mars observed by MAVEN, *Geophys. Res. Lett.*, *42*, doi:10.1002/2015GL065293.

Connerney, J. E. P., J. Espley, P. Lawton, S. Murphy, J. Odom, R. Oliversen, and D. Sheppard (2014), The MAVEN magnetic field investigation, *Space Sci. Rev.*, doi:10.1007/s11214-015-0169-4.

Crider, D. H., J. Espley, D. Brain, D. Mitchell, J. Connerney, and M. Acuña (2005), Mars Global Surveyor observations of the Halloween 2003 solar superstorm's encounter with Mars, *J. Geophys. Res.*, *110*, A09S21, doi:10.1029/2004JA010881.

Curry, S. M., M. Liemohn, X. Fang, Y. Ma, and J. Espley (2013), The influence of production mechanisms on pick-up ion loss at Mars, *J. Geophys. Res. Space Physics*, *118*, 554–569, doi:10.1029/2012JA017665.

Curry, S. M., M. Liemohn, X. Fang, Y. Ma, J. Slavin, J. Espley, S. Bougher, and C. F. Dong (2014), Test particle comparison of heavy atomic and molecular ion distributions at Mars, *J. Geophys. Res. Space Physics*, *119*, 2328–2344, doi:10.1002/2013JA019221.

Curry, S. M., J. Luhmann, Y. Ma, M. Liemohn, C. F. Dong, and T. Hara (2015), Comparative pick-up ion distributions at Mars and Venus: Consequences for atmospheric deposition and escape, *Planet. Space Sci.*, doi:10.1016/j.pss.2015.03.026.

Dong, C., et al. (2015), Multifluid MHD study of the solar wind interaction with Mars' upper atmosphere during the 8 March 2015 ICME event, *Geophys. Res. Lett.*, *42*, doi:10.1002/2015GL065944.

Dong, Y., X. Fang, D. A. Brain, J. P. McFadden,J. S. Halekas, J. E. Connerney, S. M. Curry, Y. Harada, J. G. Luhmann, and B. M. Jakosky, (2015), Strong plume fluxes at Mars observed by MAVEN: An important planetary ion escape channel, *Geophys. Res. Lett.*, *42*, doi:10.1002/2015GL065346.

Dubinin, E., M. Fraenz, A. Fedorov, R. Lundin, N. Edberg, F. Duru, and O. Vaisberg (2011), Ion energization and escape on Mars and Venus, *Space Sci. Rev.*, *162*(1–4), 173–211, doi:10.1007/s11214-011-9831-7.

Edberg, N. J. T., et al. (2011), Atmospheric erosion of Venus during stormy space weather, *J. Geophys. Res.*, *116*, A09308, doi:10.1029/2011JA016749.

Fang, X., M. W. Liemohn, A. F. Nagy, Y. Ma, D. L. De Zeeuw, J. U. Kozyra, and T. H. Zurbuchen (2008), Pickup oxygen ion velocity space and spatial distribution around Mars, *J. Geophys. Res.*, *113*, A02210, doi:10.1029/2007JA012736.

Futaana, Y., S. Barabash, A. Grigoriev, D. Winningham, R. Frahm, M. Yamauchi, and R. Lundin (2006), Global response of Martian plasma environment to an interplanetary structure: From Ena and plasma observations at Mars, *Space Sci. Rev.*, *126*(1–4), 315–332, doi:10.1007/s11214-006-9026-9.

Haider, S. A., M. A. Abdu, I. S. Batista, J. H. Sobral, E. Kallio, W. C. Maguire, and M. I. Verigin (2009), On the responses to solar X-ray flare and coronal mass ejection in the ionospheres of Mars and Earth, *Geophys. Res. Lett.*, *36*, L13104, doi:10.1029/2009GL038694.

Halekas, J. S., E. R. Taylor, G. Dalton, G. Johnson, D. W. Curtis, J. P. McFadden, D. L. Mitchell, R. P. Lin, and B. M. Jakosky (2015), The Solar Wind Ion Analyzer for MAVEN, *Space Sci. Rev.*, doi:10.1007/s11214-013-0029-z.

Jakosky, B. M., et al. (2015), MAVEN observations of the response of Mars to an interplanetary coronal mass ejection, *Science*, doi:10.1126/science.aad0210.

Leblanc, F., and R. E. Johnson (2002), Role of molecular species in pickup ion sputtering of the Martian atmosphere, *J. Geophys. Res.*, *107*(E2), 5010, doi:10.1029/2000JE001473.

Luhmann, J. G., R. E. Johnson, and M. H. G. Zhang (1992), Evolutionary impact of sputtering of the Martian atmosphere by O(+) pickup ions, *Geophys. Res. Lett.*, *19*(21), 2151–2154, doi:10.1029/92GL02485.

Leblanc, F., et al. (2015), Mars heavy ion precipitating flux as measured by MAVEN, *Geophys. Res. Lett.*, *42*, doi:10.1002/2015GL066170.

Ma, Y. J., A. F. Nagy, I. V. Sokolov, and K. C. Hansen (2004), Three-dimensional, multispecies, high spatial resolution MHD studies of the solar wind interaction with Mars, *J. Geophys. Res.*, *109*, A07211, doi:10.1029/2003JA010367.

Ma, Y. J., et al. (2015), MHD model results of solar wind interaction with Mars and comparison with MAVEN plasma observations, *Geophys. Res. Lett.*, *42*, doi:10.1002/2015GL065218.

McFadden, J., et al. (2014), The MAVEN Suprathermal and thermal Ion Composition (STATIC) Instrument, *Space Sci. Rev.*, in press.

Opgenoorth, H. J., D. J. Andrews, M. Fränz, M. Lester, N. J. T. Edberg, D. Morgan, F. Duru, O. Witasse, and A. O. Williams (2013), Mars ionospheric response to solar wind variability, *J. Geophys. Res. Space Physics*, *118*, 6558–6587, doi:10.1002/jgra.50537.

Powell, K., P. Roe, T. Linde, T. Gombosi, and D. De Zeeuw (1999), A solution-adaptive upwind scheme for ideal magnetohydrodynamics, *J. Comput. Phys.*, *154*, 284–309.

Prise, A. J., L. K. Harra, S. A. Matthews, C. S. Arridge, and N. Achilleos (2015), Analysis of a coronal mass ejection and corotating interaction region as they travel from the Sun passing Venus, Earth, Mars, and Saturn, *J. Geophys. Res. Space Physics*, *120*, 1566–1588, doi:10.1002/2014JA020256.

Rahmati, A., D. E. Larson, T. E. Cravens, R. J. Lillis, P. A. Dunn, J. S. Halekas, J. E. Connerney, F. G. Eparvier, E. M. B. Thiemann, and B. M. Jakosky, (2015), MAVEN insights into oxygen pickup ions at Mars, *Geophys. Res. Lett.*, *42*, doi:10.1002/2015GL065262.

Rouillard, A. P., et al. (2009), A solar storm observed from the Sun to Venus using the STEREO, Venus Express, and MESSENGER spacecraft, *J. Geophys. Res.*, *114*, A07106, doi:10.1029/2008JA014034.

Wang, Y.-C., J. G. Luhmann, F. Leblanc, X. Fang, R. E. Johnson, Y. Ma, W.-H. Ip, and L. Li (2014), Modeling of the O^+ pickup ion sputtering efficiency dependence on solar wind conditions for the Martian atmosphere, *J. Geophys. Res. Planets*, *119*, 93–108, doi:10.1002/2013JE004413.